

Standard and inverse site percolation of straight rigid rods on triangular lattices: Isotropic and perfectly oriented deposition and removal

L. S. Ramirez ^{1,2,*} P. M. Pasinetti,¹ W. Lebrecht ³ and A. J. Ramirez-Pastor ¹

¹*Departamento de Física, Instituto de Física Aplicada (INFAP), Universidad Nacional de San Luis-CONICET, Ejército de Los Andes 950, D5700HHW San Luis, Argentina*

²*Instituto de Física Interdisciplinaria y Sistemas Complejos (IFISC), CSIC-UIB, Campus Universitat Illes Balears, E-07122 Palma de Mallorca, Spain*

³*Departamento de Física, Universidad de La Frontera, Casilla 54-D, Temuco, Chile*



(Received 21 September 2020; revised 12 May 2021; accepted 9 June 2021; published 2 July 2021)

Numerical simulations and finite-size scaling analysis have been carried out to study standard and inverse percolation of straight rigid rods on triangular lattices. In the case of standard percolation, the lattice is initially empty. Then, linear k -mers (particles occupying k consecutive sites along one of the lattice directions) are randomly and sequentially deposited on the lattice. In the case of inverse percolation, the process starts with an initial configuration where all lattice sites are occupied by single monomers (each monomer occupies one lattice site) and, consequently, the opposite sides of the lattice are connected by nearest-neighbor occupied sites. Then the system is diluted by randomly removing sets of k consecutive monomers (linear k -mers) from the lattice. Two schemes are used for the depositing/removing process: an isotropic scheme, where the deposition (removal) of the linear objects occurs with the same probability in any lattice direction, and an anisotropic (perfectly oriented) scheme, where one lattice direction is privileged for depositing (removing) the particles. The study is conducted by following the behavior of four critical concentrations with size k : (i) [(ii)] standard isotropic[oriented] percolation threshold $\theta_{c,k}[\vartheta_{c,k}]$, which represents the minimum concentration of occupied sites at which an infinite cluster of occupied nearest-neighbor sites extends from one side of the system to the other. $\theta_{c,k}[\vartheta_{c,k}]$ is reached by isotropic[oriented] deposition of straight rigid k -mers on an initially empty lattice; and (iii) [(iv)] inverse isotropic[oriented] percolation threshold $\theta_{c,k}^i[\vartheta_{c,k}^i]$, which corresponds to the maximum concentration of occupied sites for which connectivity disappears. $\theta_{c,k}^i[\vartheta_{c,k}^i]$ is reached after removing isotropic [completely aligned] straight rigid k -mers from an initially fully occupied lattice. $\theta_{c,k}$, $\vartheta_{c,k}$, $\theta_{c,k}^i$, and $\vartheta_{c,k}^i$ are determined for a wide range of k ($2 \leq k \leq 512$). The obtained results indicate that (1) $\theta_{c,k}[\vartheta_{c,k}]$ exhibits a nonmonotonous dependence on the size k . It decreases[increases] for small particle sizes, goes through a minimum[maximum] at around $k = 11$, and finally increases and asymptotically converges towards a definite value for large segments $\theta_{c,k \rightarrow \infty} = 0.500(2)$ [$\vartheta_{c,k \rightarrow \infty} = 0.500(1)$]; (2) $\vartheta_{c,k}[\vartheta_{c,k}^i]$ depicts a monotonous behavior in terms of k . It rapidly increases[decreases] for small particle sizes and asymptotically converges towards a definite value for infinitely long k -mers $\vartheta_{c,k \rightarrow \infty} = 0.5334(6)$ [$\vartheta_{c,k \rightarrow \infty}^i = 0.4666(6)$]; (3) for both isotropic and perfectly oriented models, the curves of standard and inverse percolation thresholds are symmetric to each other with respect to the line $\theta(\vartheta) = 0.5$. Thus a complementary property is found $\theta_{c,k} + \theta_{c,k}^i = 1$ (and $\vartheta_{c,k} + \vartheta_{c,k}^i = 1$) which has not been observed in other regular lattices. This condition is analytically validated by using exact enumeration of configurations for small systems, and (4) in all cases, the critical concentration curves divide the θ space in a percolating region and a nonpercolating region. These phases extend to infinity in the space of the parameter k so that the model presents percolation transition for the whole range of k .

DOI: [10.1103/PhysRevE.104.014101](https://doi.org/10.1103/PhysRevE.104.014101)

I. INTRODUCTION

Since its introduction in the 1950s by Hammersley and Broadbent [1,2], the percolation problem has been a focal point of statistical mechanics, and it has been applied to a wide range of phenomena in physics, chemistry, biology, and materials science, where connectivity and clustering play an important role [3–16]. Percolation theory has also provided

insight into the behavior of more complicated models exhibiting phase transitions and critical phenomena [3,4,17–19].

Usually, the percolation model in a lattice is classified into two categories, namely, the site model and bond model [3]. In the site [bond] model, sites [bonds] of a lattice are randomly occupied with a probability θ or empty (unoccupied) with a probability $1 - \theta$. Nearest-neighboring occupied sites (bonds) form structures called clusters. In the limit of an infinite lattice, there is a well-defined value of θ , known as percolation threshold θ_c , at which an infinite cluster extends from one side of the system to the other. The percolation transition is then a geometrical phase transition where the critical concentration

*Author to whom correspondence should be addressed; lsramirez@unsl.edu.ar

separates a phase of finite clusters from a phase where a macroscopic, spanning, or infinite cluster is present. The exact determination of θ_c is an unsolved problem except for a few cases.

An interesting phenomenon occurs when the lattice is occupied by extended objects (objects occupying more than one lattice site). Under these conditions, the final state generated by irreversible adsorption is a disordered state (known as jamming state) in which no more objects can be deposited due to the absence of free space of appropriate size and shape [20,21]. The corresponding limiting or jamming coverage, θ_j , is less than that corresponding to close packing ($\theta_j < 1$). Thus the jamming coverage has an important role in the determination of the percolation threshold, and the interplay between jamming and percolation is relevant for the description of various deposition processes.

One of the simplest processes that produces a jamming state is the random sequential adsorption (RSA) of straight rigid k -mers (objects occupying k consecutive sites along one of the lattice directions) on infinite two-dimensional (2D) lattices. In RSA processes, particles are randomly, sequentially, and irreversibly deposited onto a substrate without overlapping each other [20–23].

In the case of straight rigid k -mers on triangular lattices, which is the focus of this article, Budinski-Petković and Kozmidis-Luburić [24] examined the kinetics of the RSA for values of k between 1 and 11 and lattice size $L = 128$. The coverage of the surface and the jamming limits was calculated by Monte Carlo simulations. The authors found that the jamming coverage decreases monotonically as the k -mer size increases. Later, Budinski-Petković *et al.* [25] investigated percolation and jamming thresholds for RSA of extended objects on triangular lattices. Numerical simulations were performed for lattices with linear size up to $L = 1000$, and objects of different sizes and shapes (linear segments; angled objects; triangles and hexagons). It was found that for elongated shapes the percolation threshold monotonically decreases, while for more compact shapes it monotonically increases with the object size. In the case of linear segments with values of k up to 20, the obtained results revealed that (1) the jamming coverage monotonically decreases with k , and tends to 0.56(1) as the length of the rods increases; (2) the percolation threshold decreases for shorter k -mers, reaches a value $\theta_c \approx 0.40$ for $k = 12$, and, it seems that θ_c does not significantly depend on k for larger k -mers; and (3) consequently, the ratio θ_c/θ_j increases with k . The effects of anisotropy [26] and the presence of defects [27] on the jamming behavior were also studied by the group of Budinski-Petković *et al.*

In the line of Refs. [24–27], three previous articles from our group [28–30] were devoted to the study of jamming and percolation of straight rigid k -mers on triangular lattices. These papers will be referred to as Papers I, II, and III, respectively. In Paper I, the results in Refs. [24,25] were extended to larger lattices and longer objects: $L/k = 100, 150, 200, 300$ and $2 \leq k \leq 128$ for jamming calculations, and $L/k = 32, 40, 50, 75, 100$ and $2 \leq k \leq 256$ for percolation analysis. The obtained results showed that the jamming coverage decreases monotonically approaching the asymptotic value of 0.5976(5) for large values of k . On the other hand, a nonmonotonic k size dependence was found for

the percolation threshold, in accordance with previous data for square lattices [31–34]. A similar behavior has also been reported for the thermalized case in isotropic dispersions, where a maximum in the percolation threshold as a function of aspect ratio has been found [35]. In addition, the complete analysis of critical exponents performed in Paper I revealed that the percolation phase transition involved in the system has the same universality class of the ordinary random percolation, regardless of the value of k considered.

In Paper II, the problem of inverse percolation by removing straight rigid k -mers from 2D triangular lattices was investigated by using numerical simulations and finite-size scaling analysis. The study of inverse percolation problem starts with an initial configuration, where all lattice sites are occupied by single monomers (each monomer occupies one lattice site) and, consequently, the opposite sides of the lattice are connected by nearest-neighbor occupied sites. Then the system is diluted by randomly removing straight rigid rods k -mers from the surface. The main objective is to obtain the maximum concentration of occupied sites (minimum concentration of empty sites) at which the connectivity disappears. This particular value of the concentration is named the inverse percolation threshold θ_c^i and determines a well-defined geometrical (second-order) phase transition in the system.

The results in Paper II, obtained for k ranging from 2 to 256, revealed that (i) the inverse percolation threshold exhibits a nonmonotonic behavior as a function of the k -mer size: it grows from $k = 1$ to $k = 10$, goes through a maximum at $k = 11$, and finally decreases again and asymptotically converges towards a definite value for large values of k ; (ii) the percolating and nonpercolating phases extend to infinity in the space of the parameter k and, consequently, the model presents percolation transition in all the ranges of k ; and (iii) the phase transition occurring in the system belongs to the standard random percolation universality class regardless of the value of k considered.

More recently, in Paper III numerical simulations were used to study the percolation behavior of aligned rigid rods of length k on 2D triangular lattices. The linear k -mers were irreversibly deposited along one of the directions of the lattice. The results, obtained for k ranging from 2 to 80, showed that the percolation threshold exhibits an increasing function when it is plotted as a function of the k -mer size. This behavior is completely different from that observed for square lattices, where the percolation threshold decreases with k [36]. In addition, an exhaustive study of critical exponents and universality was carried out, showing that the phase transition occurring in the system belongs to the standard random percolation universality class.

In this work the problem of standard and inverse percolation of straight rigid k -mers isotropically deposited on 2D triangular lattices is revisited. The most important simulation results obtained in previous papers are used as a starting point. Then, the calculations are extended to longer k -mers (up to $k = 512$) and values of k in the range [10,14], where the percolation threshold curves (standard and inverse) show a change in slope. The new calculations represent not only quantitative expansion but also a qualitative advance in the description of the percolation problem of isotropic straight rigid rods on triangular lattices. The results and conclusions

obtained here are backed by several features. First, the position of the minimum (maximum) observed in the curve of the percolation threshold (inverse percolation threshold) as a function of k is precisely determined: $k_{\min(\max)} = 11$. The accurate determination of this minimum had not been reported in the previous paper, Paper I. Second, the functionalities of the standard and inverse percolation thresholds for large values of k are established here. The obtained limit value (as $k \rightarrow \infty$) of the inverse percolation threshold improves previous estimate in Paper II. In the case of standard percolation, the results of the present study change drastically our understanding of the problem. In fact, the predictions in Paper I indicated that the percolation threshold exhibits a monotonous increasing tendency for large k 's and, consequently, that there exists a limit value $k \approx 10^4$ from which all jammed configurations are nonpercolating states (the percolation phase transition disappears). Based on more extensive numerical simulations, the new data show that the standard percolation threshold asymptotically converges towards a definite value for large segments, revealing that, in both standard and inverse problems, the percolating and nonpercolating phases extend to infinity in the space of the parameter k . This finding is a central result of our work. Third, the present study shows that the sum of standard and inverse percolation thresholds is equal to 1 for all value of k . This complementarity property has not been observed so far in other regular lattices. Fourth, simulation results are validated by exact enumeration of states for the case of dimers deposited on small cells.

The problem of aligned straight rigid k -mers deposited on (removed from) triangular lattices is also studied. The main results are listed below. First, the extension of the simulations to larger values of k (from $k = 80$ in Paper III to $k = 512$ in the present work) substantially improves the determination of the percolation threshold in the limit of $k \rightarrow \infty$. Thus the value obtained here [0.5334(6)] corrects the previously reported value in Paper III [0.582(9)]. Second, in the case of inverse percolation, the results of percolation threshold versus k are presented. Third, as in the isotropic case, the sum of standard and inverse percolation thresholds equals 1, confirming the generality of this behavior in triangular lattices. Fourth, the observed complementarity between standard and inverse percolation thresholds contributes to justify the striking increasing trend of the percolation threshold with k found in Paper III.

The rest of the paper is organized as follows. In Sec. II, standard and inverse percolation of straight rigid k -mers on 2D triangular lattices is revisited. Calculations are extended to longer objects. In addition, numerical results are supplemented by exact results for small lattices coming from a complete enumeration of configurations. The problem of percolation of aligned rigid rods is addressed in Sec. III. Finally, the conclusions are drawn in Sec. IV.

II. PERCOLATION OF STRAIGHT RIGID RODS ISOTROPICALLY DEPOSITED ON TRIANGULAR LATTICES

In this section we will revisit the percolation problem of straight rigid rods isotropically deposited on triangular lattices, this time focusing on the complementarity property of

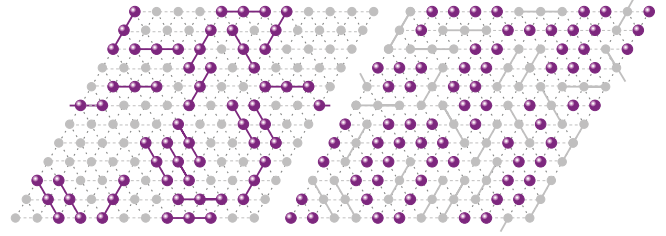


FIG. 1. (a) Schematic representation of a typical configuration obtained by isotropically depositing 3-mers ($k = 3$) on a $L \times L$ lattice with $L = 12$. Solid spheres joined by lines represent the deposited k -mers, and gray circles correspond to empty sites. (b) Schematic representation of a typical configuration obtained by removing 3-mers from an initially fully occupied $L \times L$ lattice with $L = 12$. In the full occupation state, all lattice sites are occupied by single monomers (each monomer occupies one lattice site). Solid spheres represent occupied sites (monomers), and gray circles indicate the empty sites resulting from the removal of the k -mers. Periodic boundary conditions are considered in parts (a) and (b).

the standard and inverse percolation thresholds: $\theta_c + \theta_c^i = 1$. For this purpose, new numerical simulations are presented in Sec. II A, and an analytical approach is introduced in Sec. II B.

A. Simulation results: Dependence of the standard and inverse percolation thresholds on the k -mer size

The percolation problem is defined on a 2D triangular lattice. In the computer simulations, a rhombus-shaped system of $M = L \times L$ sites (L rows and L columns) is used (see Fig. 1). Each site can be empty (hole) or occupied. Occupied and empty sites are distributed with a concentration θ and $\theta^*(= 1 - \theta)$, respectively. Nearest-neighbor occupied sites form structures called clusters, and the distribution of these sites determines the probability of the existence of a large cluster (also called an “infinite” cluster, inspired by the thermodynamic limit) that connects from one side of the lattice to the other.

Two procedures have been considered. In the first one, straight rigid k -mers (with $k \geq 2$) are deposited randomly, sequentially, and irreversibly on an initially empty lattice. This scheme, known as random sequential adsorption [21], is as follows: (i) one of the three (x_1, x_2, x_3) possible lattice directions and a starting site are randomly chosen; (ii) if, beginning at the chosen site, there are k consecutive empty sites along the direction selected in (i), then a k -mer is deposited on those sites (the k sites are marked as occupied); otherwise, the attempt is rejected. When N rods are deposited, the concentration of occupied and empty sites is $\theta = kN/M$ and $\theta^* = (M - kN)/M$, respectively.

In the second procedure, the process starts with a fully occupied lattice ($\theta = 1$ and $\theta^* = 0$). In the full occupation state, all lattice sites are occupied by single monomers (each monomer occupies one lattice site). Then the system is diluted by randomly removing groups of particles from the lattice. The mechanism of dilution is as follows: (i) a linear k -uple of k consecutive sites is chosen at random; (ii) if the k sites selected in step (i) are occupied by k particles, then a k -mer is removed from those sites. Otherwise, the attempt is rejected.

When N rods are removed, the concentration of particles (holes) is $\theta = (M - kN)/M$ ($\theta^* = kN/M$).

In both the first process (deposition) and second process (removal), periodic boundary conditions are considered. By using the first procedure (standard RSA), the lattice coverage is increased until finding a concentration at which a cluster of nearest-neighbor sites extends from one side to the opposite one of the system. This constitutes the so-called standard percolation problem, and the critical concentration rate is named standard percolation threshold.

On the other hand, when the k -mers are removed from an initially fully occupied lattice (second procedure), the fraction of occupied sites decreases until reaching a concentration at which the connectivity disappears. The model of such a process can be thought of as an inverse percolation problem. The corresponding critical concentration is then named the inverse percolation threshold. The term inverse is simply used to indicate that the size of the conductive phase diminishes during the removing process and the percolation transition occurs between a percolating and a nonpercolating state.

In the case of the jamming problem, it can be considered a mapping $L \rightarrow L^*$ from the original lattice L to the complementary lattice L^* where each empty (occupied) site of L transforms into an occupied (empty) one of L^* . Under these conditions, the filling process in the complementary lattice (dilution process in the original lattice) is equivalent to a RSA process of straight rigid k -mers. Under these conditions, standard ($\theta_{j,k}$) and inverse ($\theta_{j,k}^i$) jamming concentrations satisfy the simple expression $\theta_{j,k}^i = 1 - \theta_{j,k}$ (the supraindex i refers to the inverse problem).

The situation is more complex for the percolation problem. As discussed above, the cluster analysis for standard percolation is carried out in a phase of deposited rods. On the other hand, for inverse percolation, the cluster analysis is carried out in a phase of monomers, which remain in the lattice after the removal of a given number of straight rigid k -mers. For $k = 1$, and as a consequence of the particle-hole symmetry characterizing the usual single-particle statistics (depositing elements that occupy one single node and removing single elements), standard and inverse percolation are simply related: $\theta_{c,k=1}^i = 1 - \theta_{c,k=1}$. However, if some sort of correlation between the occupation probabilities of adjacent sites is introduced, no equivalence exists between particles and vacancies, and the mapping between standard and inverse percolation is nontrivial. To illustrate these concepts, two examples will be presented in the next paragraphs.

First, let us consider the standard percolation problem of straight rigid k -mers on square lattices. As it was shown in Ref. [34], the percolation threshold decreases for small particle sizes, goes through a minimum at around $k = 13$, and finally tends to a constant value for large k 's, $\theta_{c,k \rightarrow \infty} \approx 0.615(1)$. This behavior contrasts with the complementary case of removing straight rigid rods from square lattices [37], where the inverse percolation threshold rapidly decreases for small particle sizes ($1 \leq k \leq 3$). Then, it grows for $k = 4, 5$, and 6 , goes through a maximum at $k = 7$, and finally decreases again and asymptotically converges towards a definite value for large values of k [$\theta_{c,k \rightarrow \infty}^i \approx 0.454(4)$].

Second, let us review the classical problem of percolation of $k \times k$ square tiles deposited on square lattices. The re-

sults in Refs. [38–40] showed that the percolation threshold is an increasing function of k in the range $1 \leq k \leq 3$. For $k \geq 4$, all jammed configurations are nonpercolating states and, consequently, the percolation phase transition disappears. The inverse problem was recently investigated [41], showing that the inverse percolation threshold is a decreasing function of k in the range $1 \leq k \leq 4$ and the percolation phase transition disappears for $k \geq 5$. The marked differences between standard and inverse problems were discussed in detail in Ref. [41].

Clearly, there is no simple relationship linking standard and inverse percolation thresholds in the previous examples. These findings (and others not reviewed here) indicate that, even though the jamming properties of the standard and inverse models are trivially symmetric, the inverse percolation problem cannot be derived straightforwardly from the standard percolation problem and it deserves a detailed treatment as presented here.

Typical configurations obtained from deposition and removal procedures are shown in Figs. 1(a) and 1(b). A system with $L = 12$ and $k = 3$ is depicted in the figure. In part (a), solid spheres joined by lines represent the deposited k -mers and gray circles correspond to empty sites. In part (b), solid spheres represent occupied sites and gray circles indicate the empty sites resulting from the removal of the k -mers.

Standard and inverse percolation thresholds can be calculated by using an extrapolation method based on scaling laws [3]:

$$\theta_{c,k}(L) = \theta_{c,k} + A_k L^{-1/\nu} \quad (1)$$

and

$$\theta_{c,k}^i(L) = \theta_{c,k}^i + A_k^i L^{-1/\nu}, \quad (2)$$

where $\theta_{c,k}[\theta_{c,k}^i]$ is the standard[inverse] percolation threshold in the thermodynamic limit ($L \rightarrow \infty$) for an object of size k , A_k and A_k^i are nonuniversal constants, and ν is the critical exponent of the correlation length, which in two dimensions is $\nu = 4/3$ [3]. The quantities $\theta_{c,k}(L)[\theta_{c,k}^i(L)]$ represent the percolation thresholds for finite lattices.

A standard method to obtain $\theta_{c,k}(L)[\theta_{c,k}^i(L)]$ consists of the following steps: (a) the construction of a triangular lattice of linear size L and coverage θ , and (b) the cluster analysis using the Hoshen and Kopelman algorithm [42]. A total of r independent runs of such a two-step procedure are carried out for each lattice size L and size k . From these runs, a number r^* of them present a percolating cluster. Then a percolation probability can be defined as $R_{L,k}(\theta) = r^*/r$. In the present study, open boundary conditions are used to determine the percolation quantities.

In the case of a standard[inverse] percolation problem, $R_{L,k}(\theta)$ is an increasing[decreasing] sigmoid function of the coverage, and $\theta_{c,k}(L)[\theta_{c,k}^i(L)]$ can be obtained from the position of the inflection point of the function $R_{L,k}(\theta)$. Interested readers are referred to Papers I–III for a more complete description of the technique to determine the percolation threshold from the percolation probability functions.

By following the procedure in Eqs. (1) and (2), standard and inverse percolation thresholds were calculated for different values of k . Since one of the main objectives of this paper

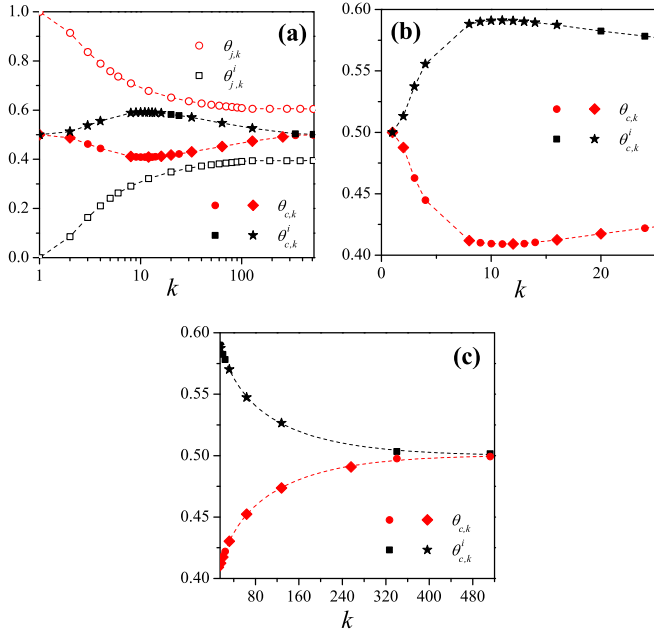


FIG. 2. (a) Standard (solid circles and solid diamonds) and inverse (solid squares and solid stars) percolation thresholds for straight rigid k -mers with k ranging between 1 and 512 on triangular lattices (k axis is presented in log scale). The figure also includes the jamming data corresponding to standard (open circles) and inverse (open squares) problems. Red (dark gray in grayscale) symbols and black symbols represent standard and inverse data. The curves were obtained by following the isotropic deposition-removal scheme. Solid diamonds and solid stars denote results from Papers I and II, respectively. Solid circles and solid squares indicate values obtained in the present work. (b) Standard and inverse percolation curves with k between 1 and 24 and with the vertical axis scaled from 0.4 to 0.6. (c) Standard and inverse percolation thresholds for values of k varying between 16 and 512. The dashed lines corresponds to the fitting curve for each system, from which we get $\theta_{c,k \rightarrow \infty} = 0.500(2)$ and $\theta_{c,k \rightarrow \infty}^i = 0.500(1)$.

is to explore the relationship between the standard and inverse percolation processes in a triangular geometry, we calculated the corresponding percolation thresholds for a broad range of k . The new values, that reach $k = 512$, also give the possibility to better establish the minimum[maximum] of the $\theta_{c,k}[\theta_{c,k}^i]$ dependence with k and to calculate the limit for $k = \infty$.

In the case of $k \leq 24$, the values of the standard and inverse percolation thresholds were obtained for lattice sizes $L/k = 32, 40, 50, 75, \text{ and } 100$. In the case of $k = 340$ and 512 , two relatively small values of L/k were used to calculate $\theta_{c,k}$ and $\theta_{c,k}^i$ ($L/k = 40$ and $L/k = 50$), with an effort reaching almost the limits of our computational capabilities. In all cases, $r = 10^5$ computational runs were performed for each concentration θ , on each lattice size L , and for each k -mer size k . The results are collected in Fig. 2: solid red (dark gray in grayscale) circles and solid black squares represent standard and inverse percolation thresholds for straight rigid k -mers on triangular lattices, respectively.

For comparison, Fig. 2 includes the values of $\theta_{c,k}$ and $\theta_{c,k}^i$ previously reported in Papers I and II, respectively: solid red (dark gray in grayscale) diamonds indicate standard per-

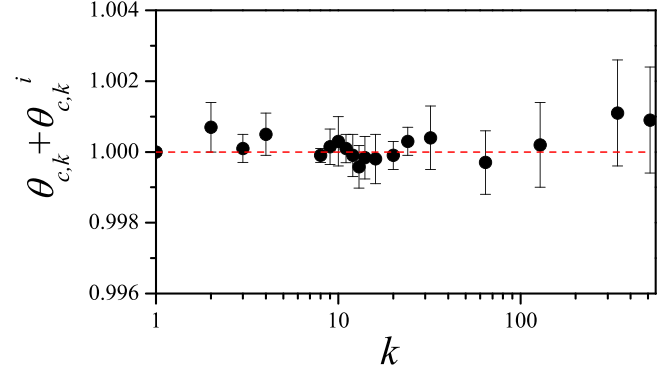


FIG. 3. The figure shows the sum of the standard and inverse percolation thresholds for the complete range of considered k sizes (note the logarithmic scale on the k axis). The values correspond to the isotropic deposition or removal problem. As it can be observed, $\theta_{c,k} + \theta_{c,k}^i = 1$.

colation thresholds and solid black stars represent inverse percolation thresholds. The figure also shows the jamming curves corresponding to standard ($\theta_{j,k}$ vs k , open circles) and inverse ($\theta_{j,k}^i$ vs k , open squares) problems [28,29].

For clarity, Fig. 2 is divided into three data groups: (a) jamming and percolation thresholds are shown in the range $1 \leq k \leq 512$ (k axis is presented in log scale). In addition to the standard and inverse percolating regions, the jamming curves in Fig. 2(a) allow one to visualize the limits of the forbidden regions of θ space; (b) percolation curves are now plotted with k between 1 and 24 and with the vertical axis scaled from 0.4 to 0.6. This vertical scale allows for a better visualization of the minimum (maximum) in the standard (inverse) percolation curve; and (c) percolation curves are shown with k ranging from $k = 16$ to $k = 512$.

As it can be observed from Fig. 2(a), the consistency between the results obtained in the present paper (solid circles and solid squares) and those previously reported in Papers I and II (solid diamonds and solid stars) is very strong. These new results complement the previous data and allow a deeper characterization of the percolation transition occurring in triangular lattices. Thus several important conclusions can be drawn from the data in Fig. 2.

First, a complementarity property between the percolation thresholds for standard and inverse percolation is found: $\theta_{c,k} + \theta_{c,k}^i = 1$. This property is exact for the case $k = 1$ [3,43] and, as shown in Fig. 3, it holds for the entire range of k , even in the limit of large values of k (note the logarithmic scale on the k axis). In the figure, both simulation percolation thresholds were summed for each k . In every case, $\theta_{c,k} + \theta_{c,k}^i = 1$ within the numerical error.

The complementarity property is a nontrivial property and seems to be strongly dependent on the topology of the lattice. As mentioned above, it is not observed for other systems, such as square [34,36–40] or honeycomb lattices [44,45]. What is more, this property was not found in square bond lattices either [46], even when triangular site lattices and square bond lattices share the same coordination number.

Secondly, the standard percolation threshold exhibits a nonmonotonous dependence on the size k [see Fig. 2(b)].

$\theta_{c,k}$ decreases for small particles sizes, goes through a minimum at around $k = 11$ [being $\theta_{c,k=11} = 0.4091(3)$], and finally increases and asymptotically converges towards a definite value for large segments. The precise determination of this minimum is reported here. In the case of inverse percolation, a maximum at $k = 11$ had been found in Paper II. This finding confirms the complementarity property discussed above.

Finally, the behavior of the percolation thresholds for large values of k [see Fig. 2(c)] indicates that both $\theta_{c,k}$ and $\theta_{c,k}^i$ tend to 0.5 for infinitely long k -mers. In fact, the simulation data can be very well fitted with the functions $a_1 \exp(-k/b_1) + a_2 \exp(-k/b_2) + a_3$ and $a_1^i \exp(-k/b_1^i) + a_2^i \exp(-k/b_2^i) + a_3^i$ for standard and inverse percolation, respectively. In this case, the adjustment was performed for $k \geq 14$. The obtained results show that $a_3 = \theta_{c,k \rightarrow \infty} = 0.500(2)$ and $a_3^i = \theta_{c,k \rightarrow \infty}^i = 0.500(1)$. In addition, $a_1 = -0.040(6)$, $a_2 = -0.073(7)$, $b_1 = 30(5)$, and $b_2 = 120(10)$ for the standard case, and $a_1^i = 0.043(9)$, $a_2^i = 0.070(9)$, $b_1^i = 34(9)$, and $b_2^i = 127(10)$ for the inverse percolation problem. As expected, the fitting curves fulfill the complementary condition $\theta_{c,k} + \theta_{c,k}^i = 1$.

The limit value obtained here $\theta_{c,k \rightarrow \infty}^i = 0.500(1)$ improves previous estimate in Paper II, where the value obtained of $\theta_{c,k \rightarrow \infty}^i$ was 0.506(2). Due to the lattice sizes used in this contribution, our present determination of $\theta_{c,k \rightarrow \infty}^i$ is expected to be more accurate than that previously reported.

As in the case of square lattices [33,34], the nonmonotonic behavior observed in the percolation curves of Fig. 2 can be interpreted as a consequence of the local alignment effects occurring for larger k (long needles) and their influence on the structure of the critical clusters. For long k -mers, the formation of $k \times k$ blocks of parallel k -mers reverses the initial decrease in $\theta_{c,k}$, leading to the appearance of a minimum in the curve of percolation threshold as a function of the size k . Even though the problem of percolation of ideal $k \times k$ blocks on triangular lattices has not yet been studied, it is expected that the percolation concentration increases with k [37–39].

To gain some understanding on the two regimes observed in $\theta_{c,k}$ and $\theta_{c,k}^i$ (below and above $k = 11$), the connectivity properties of the percolating phases were analyzed for standard and inverse percolation. Namely, for each percolation model (standard and inverse) and each value of k , the average number of occupied nearest-neighbor sites of each occupied site (normalized to the lattice size M) was measured as a function of the lattice coverage θ . We denote these functions as $\xi_k^s(\theta)$ and $\xi_k^i(\theta)$ for standard and inverse percolation, respectively.

As an example, let us consider the case of monomers distributed at random on the lattice. The function $\xi_{k=1}^s(\theta)$ can be written as $\xi_{k=1}^s(\theta) = 6\theta$, where 6 is the triangular lattice connectivity and θ is the occupation probability of each site. For $k > 1$, the statistical problem becomes more complex and it is difficult to obtain the functions $\xi_k^{s(i)}(\theta)$ analytically.

We focus now on the behavior of the connectivity of the deposited phase (clusters of occupied sites) at percolation threshold $\xi_k^s(\theta_{c,k})$ (standard percolation problem) and $\xi_k^i(\theta_{c,k}^i)$ (inverse percolation problem). In the case $k = 1$, $\xi_{k=1}^s(\theta_{c,k=1} = 0.5) = 3.0$ and $\xi_{k=1}^i(\theta_{c,k=1}^i = 0.5) = 3.0$.

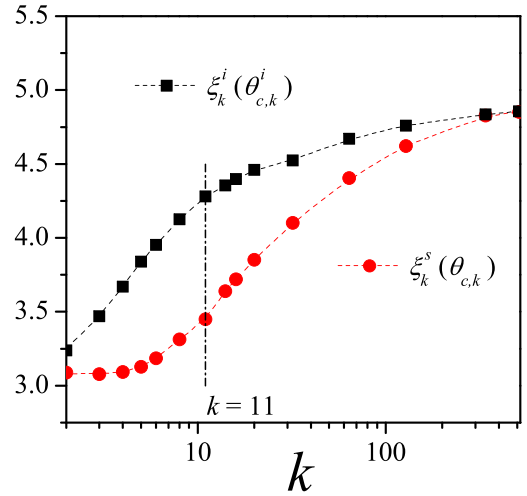


FIG. 4. Connectivity of the deposited phase at percolation threshold as a function of k . The curves were obtained by following the isotropic deposition and removal scheme. Solid circles represent results obtained for standard percolation [$\xi_k^s(\theta_{c,k})$]. Solid squares correspond to inverse percolation [$\xi_k^i(\theta_{c,k}^i)$]. The dashed lines are simply a guide for the eye. In all cases, $L/k = 340$.

$\xi_k^s(\theta_{c,k})$ (solid circles) and $\xi_k^i(\theta_{c,k}^i)$ (solid squares) as functions of k are shown in Fig. 4 for lattices with $L/k = 340$ and different values of k ranging from $k = 2$ to $k = 512$.

Let us start analyzing the behavior of $\xi_k^s(\theta_{c,k})$ versus k (solid circles in Fig. 4). The two regimes mentioned above can be clearly visualized in the curve of connectivity, which shows an inflection point at around $k = 11$. The steepest increase observed in ξ_k^s around $k = 11$ is consistent with the formation of blocks of parallel k -mers, reinforcing the hypothesis that (i) the minimum in the curve of $\theta_{c,k}$ versus k is a consequence of local alignment effects, and (ii) these blocks dominate the structure of the adsorbed phase for long k -mers. In the problem of inverse percolation (solid squares in Fig. 4), the transition between the two percolation regimes is also marked by the change in the slope of ξ_k^i around $k = 11$.

To conclude with the analysis of the connectivity, the results shown in Fig. 4 indicate that, in terms of connectivity, the structure of the percolating phase at the critical condition tends to be similar for standard and inverse percolation as $k \rightarrow \infty$. Note that $\xi_{k \rightarrow \infty}^s \approx \xi_{k \rightarrow \infty}^i \approx 4.86$. It is interesting to compare this result with that obtained for monomers. In both cases ($k = 1$ and $k \rightarrow \infty$), the percolation thresholds are similar: $\theta_{c,k=1}[\theta_{c,k=1}^i] = 0.5$ and $\theta_{c,k \rightarrow \infty}[\theta_{c,k \rightarrow \infty}^i] \approx 0.5$. However, the corresponding connectivities are very different: $\xi_{k=1}^s = \xi_{k=1}^i = 3.0$ and $\xi_{k \rightarrow \infty}^s = \xi_{k \rightarrow \infty}^i \approx 4.86$. These values indicate that the percolating phase for $k \rightarrow \infty$ is more compact than that corresponding to $k = 1$, which is expected given the formation of domains of parallel k -mers in the case of $k \rightarrow \infty$.

In the case of standard percolation, the present results reveal a similar behavior to that reported for square lattices, where the percolation threshold tends asymptotically to a definite value for infinitely long k -mers [34]. This contrasts with the predictions in Paper I, which indicated (1) an increasing

trend for $\theta_{c,k}$ at large values of k , and (2) the existence of a limit value $k \simeq 10^4$ from which all jammed configurations are nonpercolating states and, consequently, percolation would no longer occur.

The new findings in this study (especially the complementarity property discussed above) provide a more complete and precise characterization of the standard percolation problem of straight rigid rods on triangular lattices. Namely, the $\theta_{c,k}$ curve divides the space of allowed values of θ in a percolating region and a nonpercolating region. These phases extend to infinity in the space of the parameter k so that the model presents percolation transition in all the range of k . The existence of the percolation transition for the whole range of k is consistent with the behavior observed in square lattices, in which jammed configurations reached by the deposition of needles always percolate [47].

B. Exact counting of configurations on finite cells

An exact counting of configurations on finite cells was performed in order to back up the simulation predictions. This type of approach has been successfully applied to a variety of percolation problems [48–50]. Specifically, we will explore the relationship between standard and inverse thresholds from an analytical approach. The system chosen for the study was a RSA of dimers (objects occupying two consecutive lattice sites) on triangular lattices. The dimer is the simplest case of a straight rigid k -mer and contains all the properties of the multisite-occupancy deposition.

We assume that the deposition or removal of dimers takes place on a small lattice of $m = l \times l$ sites. Once deposited the dimer remains “frozen” on the substrate without dissociations or migrations. As n dimers are deposited, the coverage is $\theta = 2n/m$. On the other hand, in the inverse case, as n dimers are removed from an initially fully occupied lattice, the coverage is $\theta = 1 - 2n/m$. Thus, for any given θ , different combinations of the n dimers are possible, each one of which called a configuration.

It is useful now to define the probability $r_l^{D[l]}(n)$ that a lattice composed of $l \times l$ sites percolates at a given value of n . The index $D[l]$ in the definition of r_l indicates that n is the number of deposited[removed] dimers. Then, for each value of n , $r_l^{D[l]}$ can be obtained as the ratio between the configurations that present a percolation cluster $C_l^{D[l]}$, and the total number of ways of distributing (depositing or removing) n dimers on the $l \times l$ lattice T_l : $r_l^{D[l]} = C_l^{D[l]}/T_l$.

T_l , C_l^D , and C_l^I for different values of n are compiled in Tables I (case $l = 4$), II (case $l = 5$), and III (case $l = 6$). A C++ code was developed to exactly calculate the values in Tables I–III. The computer algorithm consists of a finite number of nested cycles through which all the possible ways of arranging n dimers on a $l \times l$ finite cell are visited and, consequently, the quantities of interest are obtained. A simplified description of the algorithm for the deposition case is presented in the next paragraph:

(1) Define and initialize the variables of the system: number of dimers n and cell size l .

(2) Generate m cycles to go through all possible ways of arranging n dimers on a $l \times l$ cell; open boundary conditions

TABLE I. Values of the quantities T_l , C_l^D , and C_l^I for 4×4 lattices.

$2n$	T_l	C_l^D	C_l^I
0	1	0	1
2	33	0	33
4	412	20	392
6	2485	585	1900
8	7664	4416	3248
10	11747	10321	1426
12	7973	7901	72
14	1802	1802	0
16	56	56	0

are used to deposit the n dimers. Two typical configurations for $n = 2$ and $l = 4$ are shown in Fig. 5.

(3) Once a new configuration is obtained, the Hoshen and Kopelman algorithm (with open boundary conditions) [42] is used to determine the existence or not of a percolating cluster. The percolating cluster is defined as a sequence of nearest-neighbor occupied sites, starting from an occupied site in the first column ($i = 1$) and ending in an occupied site in the last column ($i = 4$). Examples of nonpercolating and percolating configurations are presented in Fig. 5.

(4) At the end of the cycles, the total number of different configurations T_l and the number of percolating configurations C_l^D are recorded in a file.

A similar protocol is performed for the inverse problem. In this case, n dimers are removed from an initially fully occupied $l \times l$ cell, and the cluster analysis is carried out on the remaining $l^2 - 2n$ occupied sites. In the full occupation state, all cell sites are occupied by single monomers (each monomer occupies one cell site).

By observing Tables I–III, it is clear that $T_l(n) = C_l^D(n) + C_l^I(n)$ and, consequently, $r_l^D(n) + r_l^I(n) = 1$. This finding is further proof that $\theta_c + \theta_c^i = 1$, as found in the previous section. This property is observed only for triangular lattices. In the case of square and honeycomb lattices, $T_l(n) \neq C_l^D(n) + C_l^I(n)$ and $\theta_c + \theta_c^i \neq 1$ (data not shown here for brevity).

TABLE II. Values of the quantities T_l , C_l^D , and C_l^I for 5×5 lattices.

$2n$	T_l	C_l^D	C_l^I
0	1	0	1
2	56	0	56
4	1325	0	1325
6	17384	386	16998
8	139581	14180	125401
10	714510	192618	521892
12	2357344	1211811	1145533
14	4957616	3755572	1202044
16	6429895	5898574	531321
18	4834116	4759098	75018
20	1889380	1887961	1419
22	313128	313128	0
24	13872	13872	0

TABLE III. Values of the quantities T_l , C_l^D , and C_l^I for 6×6 lattices.

$2n$	T_l	C_l^D	C_l^I
0	1	0	1
2	85	0	85
4	3226	0	3226
6	72367	112	72255
8	1070675	11697	1058978
10	11040975	445881	10595094
12	81784784	8733484	73051300
14	442056227	99382990	342673237
16	1753845586	691161330	1062684256
18	5097923676	3000151582	2097772094
20	10757573387	8227928526	2529644861
22	16203594367	14427516941	1776077426
24	16968630295	16294784319	673845976
26	11881028004	11760742642	120285362
28	5248329234	5240762986	7566248
30	1337245213	1337175475	69738
32	169111110	169111110	0
34	7902376	7902376	0
36	56568	56568	0

III. PERCOLATION OF PERFECTLY ORIENTED STRAIGHT RIGID RODS ON TRIANGULAR LATTICES

To have a more complete insight of the percolation processes in the triangular lattice, in this section, the oriented percolation is studied with a focus in the complementary property observed in the isotropically case. For standard percolation, we reproduced and extended the results in Paper III. The results for inverse oriented percolation are reported here.

Model and basic definitions

To study the effect of k -mer alignment on percolation, straight rigid rods are deposited randomly, sequentially, and irreversibly on a $M = L \times L$ sites rhombus-shaped triangular lattice. The deposition process is performed as in Sec. II A but, now, the following restriction is considered: the k -mers are deposited along only one of the directions of the lattice. This leads to the formation of an oriented structure as depicted in Fig. 6(a). Periodic boundary conditions are considered in the deposition procedure.

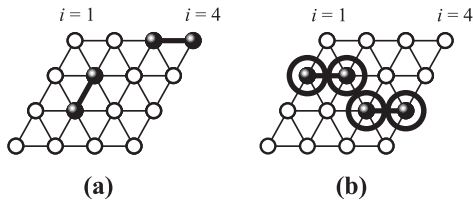


FIG. 5. Typical configurations obtained for $n = 2$ and $l = 4$. Deposited dimers and empty sites are represented by spheres joined by thick lines and open circles, respectively. $i = 1$ ($i = 4$) denotes the first(last) column in the cell. (a) Nonpercolating configuration. (b) Percolating configuration. The sites belonging to the percolating cluster are highlighted by large open circles.

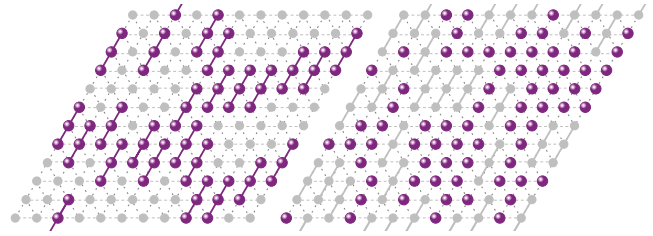


FIG. 6. (a) Schematic representation of a typical configuration obtained by perfectly oriented deposition of 3-mers ($k = 3$) on a $L \times L$ lattice with $L = 12$. Solid spheres joined by lines represent the deposited k -mers and gray circles correspond to empty sites. (b) Schematic representation of a typical configuration obtained by removing aligned 3-mers from an initially fully occupied $L \times L$ lattice with $L = 12$. In the full occupation state, all lattice sites are occupied by single monomers (each monomer occupies one lattice site). Solid spheres represent occupied sites (monomers), and gray circles indicate the empty sites resulting from the removal of the k -mers. Periodic boundary conditions are considered in parts (a) and (b).

In order to distinguish between an isotropic and oriented problem, for the rest of the paper we will use the variable ϑ to denote the concentration of occupied sites for the case of perfectly oriented deposition. It is important to note that in the present paper we treat with completely aligned states generated by irreversible adsorption of straight rigid rods. This phenomenon should not be confused with the classical nematic condition occurring in thermodynamic equilibrium. Interesting examples of percolation in equilibrium nematic states of hard rods can be found in Refs. [51,52].

The inverse percolation problem is also considered for the perfectly oriented case. We start from an initially fully occupied lattice, where all lattice sites are occupied by single monomers (each monomer occupies one lattice site). The full occupation state is diluted as follows: (1) one lattice direction $x_i \equiv \{x_1, x_2, x_3\}$ is chosen for the whole removal process; (2) a set of k consecutive nearest-neighbor sites (aligned along the selected x_i direction) is randomly chosen; and (3) if the k sites selected in step (2) are occupied, then a k -mer is removed from those sites. Otherwise, the attempt is rejected. Steps (2) and (3) are repeated until the desired number of k -mers N is removed from the lattice and the concentration of occupied particles is $\vartheta^i = (M - kN)/M$. The removal process leads to configurations as depicted in Fig. 6(b). Periodic boundary conditions are considered.

The standard and inverse percolation thresholds are obtained through the extrapolation given by Eqs. (1) and (2). In this case, the equations can be written as

$$\vartheta_{c,k}(L) = \vartheta_{c,k} + \tilde{A}_k L^{-1/\nu} \quad (3)$$

and

$$\vartheta_{c,k}^i(L) = \vartheta_{c,k}^i + \tilde{A}_k^i L^{-1/\nu}, \quad (4)$$

where \tilde{A}_k and \tilde{A}_k^i are the scaling constants for the standard and inverse perfectly oriented problem, respectively. Once the positions $\vartheta_{c,k}(L)$ and $\vartheta_{c,k}^i(L)$ are determined from the percolation probability functions $R_{L,k}(\vartheta)$, the percolation thresholds

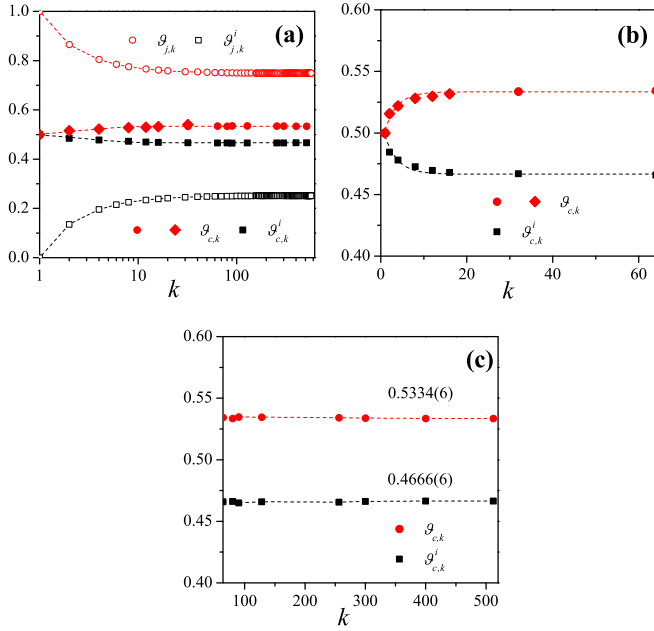


FIG. 7. (a) Standard (solid circles and solid diamonds) and inverse (solid squares) percolation thresholds for straight rigid k -mers, with k ranging between 1 and 512 on triangular lattices (k axis is presented in log scale). The figure also includes the jamming data corresponding to standard (open circles) and inverse (open squares) problems. Red (dark gray in grayscale) symbols and black symbols represent standard and inverse data. The curves were obtained by following the perfectly oriented deposition and removal scheme. Solid diamonds denote results from Paper III, respectively. Solid circles and solid squares indicate values obtained in the present work. (b) Standard and inverse percolation thresholds for values of k varying between 1 and 64 and with the vertical axis scaled from 0.4 to 0.6. (c) Standard and inverse percolation thresholds for values of k varying between 64 and 512. The dashed lines correspond to the fitting curve for each system, from which we get that $\theta_{c,k \rightarrow \infty} = 0.5334(6)$ and $\theta^i_{c,k \rightarrow \infty} = 0.4666(6)$.

$\vartheta_{c,k}$ and $\vartheta^i_{c,k}$ can be obtained using the extrapolation scheme in Eqs. (3) and (4).

The obtained curves for $\vartheta_{c,k}$ and $\vartheta^i_{c,k}$ as functions of size k are shown in Fig. 7. As in the case of Fig. 2, the data are divided into three groups: (a) Percolation thresholds are shown in the range $1 \leq k \leq 512$. The k axis is presented in log scale, and the vertical axis ranges from 0 to 1. (b) Percolation curves are now plotted with k between 1 and 64 and with the vertical axis scaled from 0.4 to 0.6. (c) Percolation curves are shown with k ranging from $k = 64$ to $k = 512$. Solid red (dark gray in grayscale) symbols and solid black symbols represent standard and inverse percolation thresholds, respectively. Figure 7(a) includes the jamming curves corresponding to standard ($\vartheta_{j,k}$ vs k , open circles) and inverse ($\vartheta^i_{j,k}$ vs k , open squares) problems.

For k between 2 and 32 lattices sizes $L/k = 128, 256, 384, 512$, and 640 were considered; for k between 64 and 90 $L/k = 32, 64, 128, 200$, and 256; and for higher values of k , $k = 128, 256, 300, 400, 512$, $L/k = 50$ up to $L/k = 150$. For $\vartheta_{c,k}$, the values obtained in the present work (solid circles) are consistent with those reported in Paper III

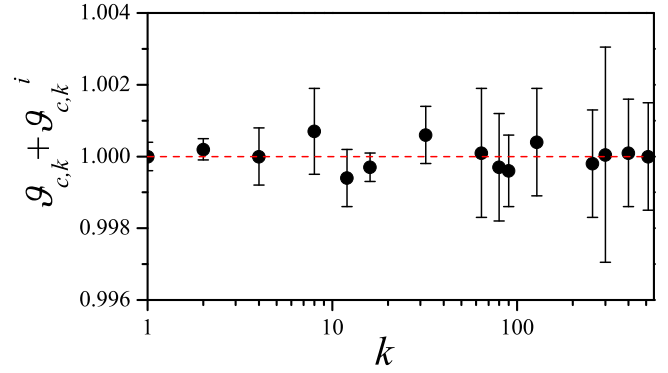


FIG. 8. Sum of the standard and inverse percolation thresholds for all the range of considered k sizes (note the logarithmic scale on the k axis). The values correspond to the perfectly oriented deposition problem. As it can be observed, $\theta_{c,k} + \theta^i_{c,k} = 1$.

[53] (solid diamonds). On the other hand, in the case of the inverse percolation problem, the behavior of $\vartheta^i_{c,k}$ in terms of k is reported here (solid squares in Fig. 7).

The curves of standard and inverse percolation thresholds are symmetric to each other with respect to the line $\vartheta = 0.5$. As in the isotropic percolation problem, $\vartheta_{c,k} + \vartheta^i_{c,k} = 1$ within the numerical error and, accordingly, the complementarity property is also valid for the perfectly oriented percolation problem. The sum $\theta_{c,k} + \theta^i_{c,k}$ is shown in Fig. 8 for the whole range of k values studied here (note the logarithmic scale on the k axis).

The standard and inverse percolation thresholds show a monotonous dependence on the size k . $\vartheta_{c,k}[\vartheta^i_{c,k}]$ rapidly increases[decreases] for small particles sizes and asymptotically converges towards a definite value for large segments [see Fig. 7(b)]. The behavior of the inverse percolation threshold $\vartheta^i_{c,k}$ as a function of k is reported here.

The numerical data can be very well fitted with the functions $\tilde{a}_1 \exp(-k/\tilde{b}_1) + \tilde{a}_2$ and $\tilde{a}'_1 \exp(-k/\tilde{b}'_1) + \tilde{a}'_2$ for standard and inverse percolation, respectively. The obtained results show that $\tilde{a}_2 = \vartheta_{c,k \rightarrow \infty} = 0.5334(6)$ and $\tilde{a}'_2 = \vartheta^i_{c,k \rightarrow \infty} = 0.4666(6)$ [see Fig. 7(c)]. In addition, $\tilde{a}_1 = -0.049(4)$, and $\tilde{b}_1 = 2.8(4)$ for the standard case and $\tilde{a}'_1 = 0.043(3)$, and $\tilde{b}'_1 = 3.0(5)$ for the inverse percolation problem. These findings indicate that the RSA model of aligned k -mers on triangular lattices presents standard and inverse percolation transition in the whole range of k . As expected, the fitting curves satisfy the complementary condition $\vartheta_{c,k} + \vartheta^i_{c,k} = 1$.

The limit value obtained here $\vartheta_{c,k \rightarrow \infty} = 0.5334(6)$ improves the previous estimate in Paper III [$\vartheta_{c,k \rightarrow \infty} = 0.582(9)$], where the standard perfectly oriented percolation threshold was calculated in the range $2 \leq k \leq 80$. The extension of the calculations to larger particles (in this case, up to $k = 512$) led to a new and more accurate determination of $\vartheta_{c,k \rightarrow \infty}$.

The study of connectivity in Fig. 4 was repeated for the case of perfectly oriented percolation. The results are shown in Fig. 9. Solid circles represent results obtained for standard percolation [$\xi_k^s(\vartheta_{c,k})$], and solid squares correspond to inverse

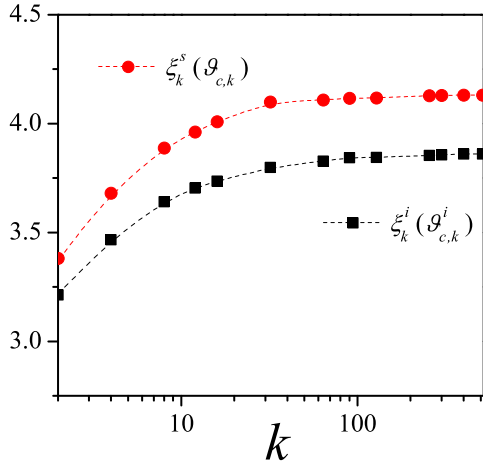


FIG. 9. Connectivity of the deposited phase at percolation threshold as a function of k . The curves were obtained by following the perfectly oriented deposition and removal scheme. Solid circles represent results obtained for standard percolation [$\xi_k^s(\vartheta_{c,k}^s)$]. Solid squares correspond to inverse percolation [$\xi_k^i(\vartheta_{c,k}^i)$]. The dashed lines are simply a guide for the eye. In all cases, $L/k = 340$.

percolation [$\xi_k^i(\vartheta_{c,k}^i)$]. In this case, the connectivity curves increase monotonously with increasing size k , asymptotically tending to a constant value as $k \rightarrow \infty$: $\xi_{k \rightarrow \infty}^s \approx 4.13$ and $\xi_{k \rightarrow \infty}^i \approx 3.86$. Thus, for long k -mers, the connectivity at the critical condition for standard percolation is greater than the one corresponding to inverse percolation ($\xi_{k \rightarrow \infty}^s > \xi_{k \rightarrow \infty}^i$), following the tendency observed for the percolation thresholds ($\vartheta_{c,k \rightarrow \infty}^s > \vartheta_{c,k \rightarrow \infty}^i$). In addition, the smooth behavior

shown in Fig. 9 contrasts with the two regimes observed in the isotropic case and is consistent with the monotonous behavior of the percolation curves in Fig. 7 (perfectly oriented percolation).

Returning to the percolation threshold curves, it is important to note that, for all k , the inverse percolation threshold of isotropic rods is higher than the corresponding one to aligned k -mers [see Fig. 10(a)]. This is of interest since it means that is easier to disconnect the system when the needles are isotropically removed. In other words, the system is more robust when the removed needles are aligned in only one direction. This finding is consistent with the behavior observed for the standard percolation problem, in which the curve for perfectly oriented percolation is considerably above than the isotropic one in the whole range of k [see Fig. 10(b)]. Theoretical and experimental work support these predictions [54–57].

IV. CONCLUSIONS

In this paper, standard and inverse percolation properties of straight rigid k -mers on triangular lattices were studied by numerical simulations and finite-size scaling analysis. Two models have been addressed: an isotropic model, where the deposition (removal) of the linear objects occurs with the same probability in any lattice direction; and a perfectly oriented model, where one lattice direction is privileged for depositing (removing) the particles.

For the isotropic deposition-removal problem, the previously reported results in Papers I and II were extended to longer k -mers (up to $k = 512$). The standard and inverse percolation thresholds exhibit a nonmonotonous dependence on the size k . $\theta_{c,k}[\theta_{c,k}^i]$ decreases[increases] for small particles sizes, goes through a minimum[maximum] at around $k = 11$, and finally increases and asymptotically converges towards a definite value for large segments.

The nonmonotonic behavior observed in the percolation curves was discussed in terms of the local alignment effects occurring in the deposited layer for large k . Based on calculations of the connectivity of the deposited phase at percolation threshold, the influence of these alignment effects on the structure of the critical clusters was analyzed. The obtained results are consistent with previous findings in square lattices [37–39], showing that, for long k -mers, the formation of $k \times k$ blocks of parallel k -mers reverses the initial decrease in $\theta_{c,k}$, leading to the appearance of a minimum in the curve of the standard percolation threshold as a function of size k . However, further research is necessary to confirm or discard this hypothesis for the case of triangular lattices. Along this line, the problem of jamming and percolation for deposition of $k \times k$ blocks on triangular lattices will be the object of future work.

For large values of k (after the minimum or maximum), the numerical data can be well fitted by the following functions: $\theta_{c,k} = a_1 \exp(-k/b_1) + a_2 \exp(-k/b_2) + a_3$ and $\theta_{c,k}^i = a_1^i \exp(-k/b_1^i) + a_2^i \exp(-k/b_2^i) + a_3^i$ ($k \geq 14$), being $a_1 = -0.040(6)$, $a_2 = -0.073(7)$, $a_3 = \theta_{c,k \rightarrow \infty} = 0.500(2)$, $b_1 = 30(5)$, $b_2 = 120(10)$, and $a_3^i = \theta_{c,k \rightarrow \infty}^i = 0.500(1)$.

The results obtained here allow us (1) to precisely determine the position of the minimum (maximum) observed in the curve of $\theta_c(\theta_c^i)$, located in $k = 11$; (2) to establish the

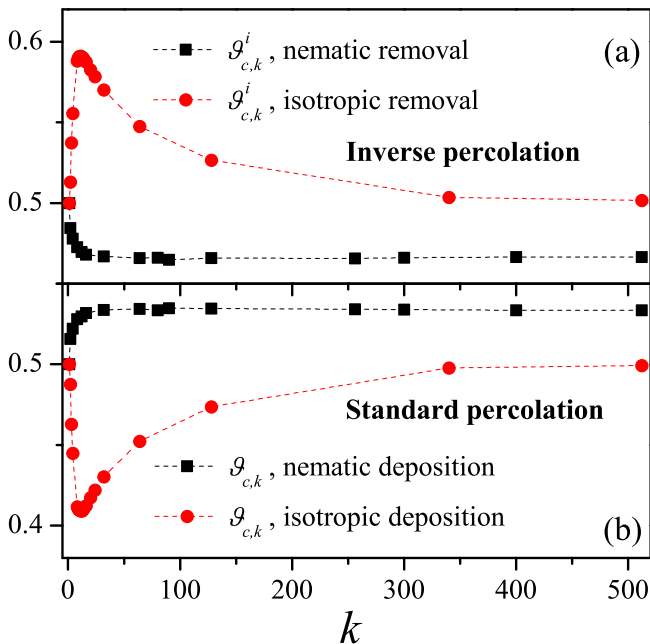


FIG. 10. (a) Comparison between isotropic (circles) and oriented (squares) percolation thresholds for the inverse percolation problem of straight rigid k -mers on triangular lattices. (b) Same as part (a) but for the standard percolation problem.

limit values $\theta_{c,k \rightarrow \infty} = 0.500(2)$ and $\theta_{c,k \rightarrow \infty}^i = 0.500(1)$, and in the case of an inverse problem, the present result corrects the previously reported value of $\theta_{c,k \rightarrow \infty}^i = 0.506(2)$ [29]; and (3) to conclude that $\theta_c + \theta_c^i = 1$ for all value of k , even for infinitely long k -mers. This complementarity property was also validated by exact counting of configurations of dimers on finite cells.

The new findings provide a more complete and precise characterization of the percolation problem of straight rigid rods on triangular lattices. As occurs in the case of square lattices [34,47], the $\theta_{c,k}$ curve divides the space of allowed values of θ in a percolating region and a nonpercolating region. These phases extend to infinity in the space of the parameter k so that the model presents a percolation transition in the entire range of k . This contrasts with the predictions in Paper I, which indicated the existence of a limit value $k \simeq 10^4$ from which all jammed configurations are nonpercolating states and, consequently, the percolation transition is missed.

Regarding the perfectly oriented case, the problem of aligned straight rigid k -mers deposited on triangular lattices was also revisited and extended. A increasing behavior was observed for $\vartheta_{c,k}$, with a finite value of saturation in the limit of infinitely long k -mers: $\vartheta_{c,k} = \tilde{a}_1 \exp(-k/\tilde{b}_1) + \tilde{a}_2$, being $\tilde{a}_1 = -0.049(4)$, $\tilde{b}_1 = 2.8(4)$, and $\tilde{a}_2 = \vartheta_{c,k \rightarrow \infty} = 0.5334(6)$. This limit value improves the previous estimate in Paper III [$\vartheta_{c,k \rightarrow \infty} = 0.582(9)$], where the standard perfectly oriented percolation threshold was calculated in the range $2 \leq k \leq 80$.

In the case of inverse percolation by removing aligned k -mers from triangular lattices, the results of $\vartheta_{c,k}^i$ in terms of size k are presented: $\vartheta_{c,k}^i = \tilde{a}_1^i \exp(-k/\tilde{b}_1^i) + \tilde{a}_2^i$, with $\tilde{a}_1^i = 0.043(3)$, $\tilde{b}_1^i = 3.0(5)$, and $\tilde{a}_2^i = \vartheta_{c,k \rightarrow \infty}^i = 0.4666(6)$.

In both standard and inverse perfectly oriented problems, the connectivity curves vary smoothly with increasing size k , which is consistent with the monotonic behavior observed in the percolation curves. The obtained results indicate the

existence of percolation phase transition in the whole range of k . In addition, and as in the isotropic case, the sum of standard and inverse percolation thresholds equals 1 ($\vartheta_{c,k} + \vartheta_{c,k}^i = 1$) for all values of k , confirming the generality of this behavior in triangular lattices. Thus the simple complementarity relationship between standard and inverse percolation thresholds seems to be a property typical for the triangular lattice, regardless of isotropic or oriented deposition or removal. The complementarity property has not been observed in other regular lattices, showing that the lattice structure plays a fundamental role in determining the statistics and percolation properties of extended objects.

Finally, it was found that, for all k , the inverse percolation threshold of isotropic rods is higher than the corresponding one to aligned k -mers. This means that the phase of occupied sites is more robust when the removed sets of sites are aligned in only one lattice direction. A contrary behavior has been theoretically and experimentally observed for the standard percolation problem, where the curve for oriented percolation is above the isotropic one in the whole range of k [53–56].

Future efforts will be dedicated to developing an analytical framework for evaluating the percolation properties of aligned rigid rods. In this case, the depositions along the director axis are fully independent, and the RSA of straight rigid rods on a one-dimensional line has been exactly solved analytically [58–61].

ACKNOWLEDGMENTS

This work was supported in part by CONICET (Argentina) under Project No. PIP 112-201701-00673CO and Universidad Nacional de San Luis (Argentina) under Project No. 03-0816. W.L. is thankful for support from Dirección de Investigación Universidad de La Frontera (Chile) under Project DIUFRO, Grant No. DI20-0007. L.S.R. acknowledges the support through the Maria de Maeztu Program for units of Excellence in R&D (MDM-2017-0711).

-
- [1] J. M. Hammersley and K. W. Morton, *J. R. Stat. Soc.* **16**, 23 (1954).
 - [2] S. R. Broadbent and J. M. Hammersley, *Proc. Cambridge Philos. Soc.* **53**, 629 (1957).
 - [3] D. Stauffer and A. Aharony, *Introduction to Percolation Theory* (Taylor & Francis, London, 1994).
 - [4] M. Sahimi, *Applications of Percolation* (Theory Taylor & Francis, London, 1994).
 - [5] S. N. Dorogovtsev and J. F. F. Mendes, *Evolution of Networks: From Biological Nets to the Internet and WWW* (Oxford University Press, Oxford, UK, 2003).
 - [6] M. E. J. Newman, A.-L. Barabási, and D. J. Watts, *The Structure and Dynamics of Networks* (Princeton University Press, New Jersey, 2006).
 - [7] M. E. J. Newman, *Networks: An Introduction* (Oxford University Press, Oxford, UK, 2010).
 - [8] R. Cohen and S. Havlin, *Complex Networks, Structure, Robustness and Function* (Cambridge University Press, Cambridge, 2010).
 - [9] Y. Kornbluth, S. Lowinger, G. A. Cwilich, and S. V. Buldyrev, *Phys. Rev. E* **89**, 032808 (2014).
 - [10] S. Lowinger, G. A. Cwilich, and S. V. Buldyrev, *Phys. Rev. E* **94**, 052306 (2016).
 - [11] Z. Gao and Z. R. Yang, *Physica A* **255**, 242 (1998).
 - [12] A. Coniglio, *J. Phys.: Condens. Matter* **13**, 9039 (2001).
 - [13] E. Kenah and J. M. Robins, *Phys. Rev. E* **76**, 036113 (2007).
 - [14] A. Yazdi, H. Hamzhepour, and M. Sahimi, *Phys. Rev. E* **84**, 046317 (2011).
 - [15] A. P. Chatterjee, *J. Chem. Phys.* **140**, 204911 (2014).
 - [16] Y. Y. Tarasevich, N. I. Lebovka, I. V. Vodolazskaya, A. V. Eserkepov, V. A. Goltseva, and V. V. Chirkova, *Phys. Rev. E* **98**, 012105 (2018).
 - [17] G. Grimmett, *Percolation* (Springer-Verlag, Berlin, 1999).
 - [18] K. Christensen and N. R. Moloney, *Complexity and Criticality* (Imperial College Press, London, 2005).
 - [19] B. Bollobás and O. Riordan, *Percolation* (Cambridge University Press, New York, 2006).
 - [20] J. Feder, *J. Theor. Biol.* **87**, 237 (1980).

- [21] J. W. Evans, *Rev. Mod. Phys.* **65**, 1281 (1993).
- [22] A. Cadilhe, N. A. M. Araújo, and V. Privman, *J. Phys.: Condens. Matter* **19**, 065124 (2007).
- [23] N. A. M. Araújo and A. Cadilhe, *J. Stat. Mech.* (2010) P02019.
- [24] L. Budinski-Petković and U. Kozmidis-Luburić, *Phys. Rev. E* **56**, 6904 (1997).
- [25] L. Budinski-Petković, I. Lončarević, M. Petković, Z. M. Jakšić, and S. B. Vrhovac, *Phys. Rev. E* **85**, 061117 (2012).
- [26] L. Budinski-Petković, I. Lončarević, Z. M. Jakšić, S. B. Vrhovac, and N. M. Švrakić, *Phys. Rev. E* **84**, 051601 (2011).
- [27] L. Budinski-Petković, I. Lončarević, Z. M. Jakšić, and S. B. Vrhovac, *J. Stat. Mech.* (2016) 053101.
- [28] E. J. Perino, D. A. Matoz-Fernandez, P. M. Pasinetti, and A. J. Ramirez-Pastor, *J. Stat. Mech.* (2015) P10011.
- [29] L. S. Ramirez, P. M. Centres, and A. J. Ramirez-Pastor, *J. Stat. Mech.* (2017) 113204.
- [30] P. Longone, P. M. Centres, and A. J. Ramirez-Pastor, *Phys. Rev. E* **100**, 052104 (2019).
- [31] Y. Leroyer and E. Pommiers, *Phys. Rev. B* **50**, 2795 (1994).
- [32] G. Kondrat and A. Pękalski, *Phys. Rev. E* **63**, 051108 (2001).
- [33] Y. Y. Tarasevich, N. I. Lebovka, and V. V. Laptev, *Phys. Rev. E* **86**, 061116 (2012).
- [34] M. G. Slutskiĭ, L. Y. Barash, and Y. Y. Tarasevich, *Phys. Rev. E* **98**, 062130 (2018).
- [35] T. Schilling, M. A. Miller, and P. van der Schoot, *Europhys. Lett.* **111**, 56004 (2015).
- [36] L. S. Ramirez, P. M. Centres, and A. J. Ramirez-Pastor, *J. Stat. Mech.* (2015) P09003.
- [37] M. Nakamura, *J. Phys. A: Math. Gen.* **19**, 2345 (1986).
- [38] M. Nakamura, *Phys. Rev. A* **36**, 2384 (1987).
- [39] A. J. Ramirez-Pastor, P. M. Centres, E. E. Vogel, and J. F. Valdés, *Phys. Rev. E* **99**, 042131 (2019).
- [40] L. S. Ramirez, P. M. Centres, and A. J. Ramirez-Pastor, *Phys. Rev. E* **100**, 032105 (2019).
- [41] P. Longone, P. M. Centres, and A. J. Ramirez-Pastor, *Phys. Rev. E* **85**, 011108 (2012).
- [42] J. Hoshen and R. Kopelman, *Phys. Rev. B* **14**, 3438 (1976).
- [43] M. F. Sykes and J. W. Essam, *J. Math. Phys.* **5**, 1117 (1964).
- [44] L. S. Ramirez, P. M. Centres, A. J. Ramirez-Pastor, and W. Lebrecht, *J. Stat. Mech.* (2019) 113205.
- [45] G. A. Iglesias Panuska, P. M. Centres, and A. J. Ramirez-Pastor, *Phys. Rev. E* **102**, 032123 (2020).
- [46] L. S. Ramirez, P. M. Centres, and A. J. Ramirez-Pastor, *Phys. Rev. E* **97**, 042113 (2018).
- [47] G. Kondrat, Z. Koza, and P. Brzeski, *Phys. Rev. E* **96**, 022154 (2017).
- [48] W. Lebrecht, J. F. Valdés, E. E. Vogel, F. Nieto, and A. J. Ramirez-Pastor, *Physica A* **392**, 149 (2013).
- [49] W. Lebrecht, J. F. Valdés, E. E. Vogel, F. Nieto, and A. J. Ramirez-Pastor, *Physica A* **398**, 234 (2014).
- [50] W. Lebrecht, E. E. Vogel, J. F. Valdés, A. J. Ramirez-Pastor, P. M. Centres, M. I. González, and F. D. Nieto, *Phys. Rev. E* **92**, 012129 (2015).
- [51] S. P. Finner, T. Schilling, and P. van der Schoot, *Phys. Rev. Lett.* **122**, 097801 (2019).
- [52] S. P. Finner, A. Atashpendar, T. Schilling, and P. van der Schoot, *Phys. Rev. E* **100**, 062129 (2019).
- [53] F. Du, J. E. Fischer, and K. I. Winey, *Phys. Rev. B* **72**, 121404(R) (2005).
- [54] N. Grossiord, J. Loos, O. Regev, and C. E. Koning, *Chem. Mater.* **18**, 1089 (2006).
- [55] H. Deng, R. Zhang, E. Bilotti, J. Loos, and T. Peijs, *J. Appl. Polym. Sci.* **113**, 742 (2009).
- [56] R. Taherian, *Compos. Sci. Technol.* **123**, 17 (2016).
- [57] R. H. Swendsen, *Phys. Rev. A* **24**, 504 (1981).
- [58] E. Ben-Naim and P. L. Krapivsky, *J. Phys. A* **27**, 3575 (1994).
- [59] N. O. Wolf, J. W. Evans, and D. K. Hoffman, *J. Math. Phys. (NY)* **25**, 2519 (1984).
- [60] A. Rényi, *Sel. Transl. Math. Stat. Probab.* **4**, 203 (1963). [translation from *Magyar Tud. Akad. Mat. Kutató Int. Közl.* **3**, 109 (1958)].
- [61] Previously published results for $k = 32$ and $k = 80$ are not shown in Fig. 7, and were replaced by new values calculated using a better statistics.